Available online at www.sciencedirect.com
ScienceDirect
Cement and Concrete Research 37 (2007) 1571–1582
Cement and Concrete Research

Composition, morphology and nanostructure of C–S–H in white Portland cement pastes hydrated at 55 °C

A.V. Girão [a], I.G. Richardson [a,*], C.B. Porteneuve [b], R.M.D. Brydson [c]

[a] School of Civil Engineering, University of Leeds, Leeds LS2 9JT, United Kingdom
[b] W.R. Grace and Company, 62 Whittemore Avenue, Cambridge, MA 02140, USA
[c] Institute for Materials Research, University of Leeds, Leeds LS2 9JT, United Kingdom

Received 15 March 2007; accepted 3 September 2007

Abstract

The C–S–H present in water- and alkali-activated hardened pastes of white Portland cement hydrated at 55 °C has been characterized. The mean length of the aluminosilicate anions in the C–S–H was similar in both systems and increased with age. Inner product C–S–H generally had a fine scale, homogeneous morphology. Outer product C–S–H was generally fibrillar with water, and foil- or lath-like with alkali. There were some regions of C–S–H with coarse morphology. It was not possible to determine the chemical composition of C–S–H using the SEM; TEM–EDX was necessary. The C–S–H formed in the alkali-activated paste had a lower mean Ca/(Al+Si) ratio than that formed with water, which was offset by a larger quantity of calcium hydroxide. The potassium in the KOH-activated paste was present either within the C–S–H structure charge balancing the substitution of Al^{3+} for Si^{4+}, or adsorbed on the C–S–H charge balancing sulfate ions.

Keywords: Portland cement; C–S–H; Temperature; TEM; NMR

1. Introduction

The reaction between cement and water leads to the formation of a number of hydration products including an amorphous or poorly crystalline calcium silicate hydrate (C–S–H), calcium hydroxide (CH) and calcium aluminate/aluminoferrite hydrate phases (AFm and AFt-type phases). C–S–H is the main binding phase in all Portland cement-based systems. As a consequence, the physical properties of a hardened cement paste are influenced strongly by the morphology and composition of the C–S–H, which are affected by many factors such as the composition of the cement, the solution/solid ratio, curing temperature, degree of hydration and the presence of chemical admixtures and supplementary cementing materials (SCM) [1]. The temperature of curing has a significant impact on the development of the physical properties of a cement paste because it affects the kinetics of hydration and the distribution and nature of the hydration products [e.g. [2–11]]. Understanding the effects of high temperatures on cement hydration (i.e. <100 °C at atmospheric pressure) is relevant in a number of situations in practice, including hot weather climates, accumulated heat evolution, and heat curing to accelerate strength gain (e.g. in precast products). The aim of this work was to determine the effect of curing at 55 °C on the composition, morphology and nanostructure of C–S–H formed in neat Portland cement pastes activated with either distilled water or 5 M KOH solution. KOH solution was used to activate one of the pastes because the resulting C–S–H is structurally better ordered than that formed with water activation. This increased order results in narrower linewidths in solid-state ^{29}Si magic angle spinning nuclear magnetic resonance (MAS NMR) spectra. Individual peaks are consequently much better resolved, which makes deconvolution of the spectra relatively straightforward. The results of the deconvolution of the NMR spectra for the KOH-activated pastes are then used to facilitate the deconvolution of the spectra for those activated with water, as in previous work on blends involving blast-furnace slag [12,13] and metakaolin

* Corresponding author. Tel.: +44 113 343 2331; fax: +44 113 343 2665.
E-mail address: I.G.Richardson@leeds.ac.uk (I.G. Richardson).

0008-8846/$ - see front matter © 2007 Elsevier Ltd. All rights reserved.
doi:10.1016/j.cemconres.2007.09.001

Table 1
Bulk oxide composition for the WPC determined by XRF

Oxides (%)	WPC
SiO_2	24.81
Al_2O_3	2.35
Fe_2O_3	0.49
MgO	0.80
CaO	68.61
Na_2O	0.15
SO_3	2.03
K_2O	0.06

[14]. Pastes were examined at 1 day and 28 days using solid-state ^{29}Si MAS NMR, backscattered electron imaging with energy dispersive X-ray analysis (EDX), thermal analysis with evolved gas analysis, and X-ray diffraction (XRD); the 28-day-old samples were also examined by transmission electron microscopy (TEM) with EDX analysis.

2. Experimental procedure

Neat white Portland cement (WPC; Castle Cement Limited, Clitheroe, U.K.) pastes were hand mixed to a water or solution to solid ratio of 0.5 (ml/g), with distilled water or with a 5 M KOH solution (referred to in the tables in this article as 'Wwpc' and 'Kwpc' respectively). The oxide composition for the anhydrous WPC obtained by X-ray fluorescence spectroscopy (XRF) is given in Table 1. The samples were cast in 7 ml polystyrene tubes, sealed in plastic bags and cured in a water bath at 55±1 °C.

XRD measurements were performed using a Panalytical X'PERT-PRO diffractometer system (with X'Celerator real time multiple strip detector), operated with Cu Kα radiation at 40 mA and 45 kV. The samples were demoulded, sliced using a slow-speed cut-off saw and mounted on a sample holder that was spun at 2 revolutions per second. XRD acquisition was carried out in continuous scan mode over the range 6.03 to 54.95 °2θ with a step width of 0.01675° (i.e. 2921 steps) and a counting time of 34.29 s, corresponding to a total acquisition time of nearly 14 min.

The quantity of calcium hydroxide in the pastes was determined by thermogravimetric analysis (STA1500, Stanton Redcroft, London, U.K.). Samples were freshly crushed and ground to a powder in an agate mortar, and were heated to 1000 °C at 20 °C/min, under a constant flow of nitrogen. An evolved gas analysis (EGA) system (Cirrus mass spectrometer, MKS Spectra Products Ltd., U.K.) interfaced with the STA equipment was used to differentiate mass loss associated with water or carbon dioxide: in fact, CO_2 was not detected in any of the samples thus confirming that no carbonation occurred during sample preparation.

Solid-state ^{29}Si single-pulse and ^{1}H–^{29}Si cross-polarization MAS NMR spectra were acquired using a Varian InfinityPlus 300 spectrometer (magnetic field 7.05T; operating frequency of 59.5 MHz for ^{29}Si). Paste samples were freshly ground after 1 day and 28 days hydration. Samples were packed into 6 mm zirconia rotors sealed at either end with Teflon end plugs, and spun at 6 kHz in a Chemagnetics-style probe. The spectra were acquired over 10000 scans using a pulse recycle delay of 2 or 5 s, a pulse width 2 or 4 μs, and an acquisition time 20 ms. Quantitative information on the fractions of Si present in silicate tetrahedra with different connectivities was obtained by deconvolution of the single-pulse spectra. In this work, the spectra were fitted using a procedure that involves the subtraction of a contribution from a spectrum taken from anhydrous cement, which thus accounted for the unreacted alite and some of the belite, followed by the iterative fitting of the remaining belite and hydrate peaks to Voigt lineshapes using IgorPro 5.0 (Wavemetrics, Inc., U.S.A.) [14]. The mean aluminosilicate chain length and the mean Al/Si ratio were calculated from the NMR data using Eqs. (1) and (2) in [15].

For scanning electron microscopy with energy dispersive X-ray analysis (SEM–EDX), the samples were demoulded and cut into 400 μm thick slices, using a slow speed cut off saw with a diamond wafering blade. The samples were dried by solvent exchange with propan-2-ol. The slices were then impregnated with epoxy–resin (Epofix Kit, Struers) under vacuum and, after hardening, polished to a flat surface on a rotary grinding/polishing machine (PdM-Force20 mounted on Struers Rotopol-35), using silicon carbide paper of different grades (600–2400 grit from Struers, Glasgow, UK). The samples were subsequently polished with diamond paste (3, 1 and 0.25 μm). The surface of the polished samples was carbon coated in a vacuum coating unit (EMSCOPE TB500, U.K.) and analyzed in

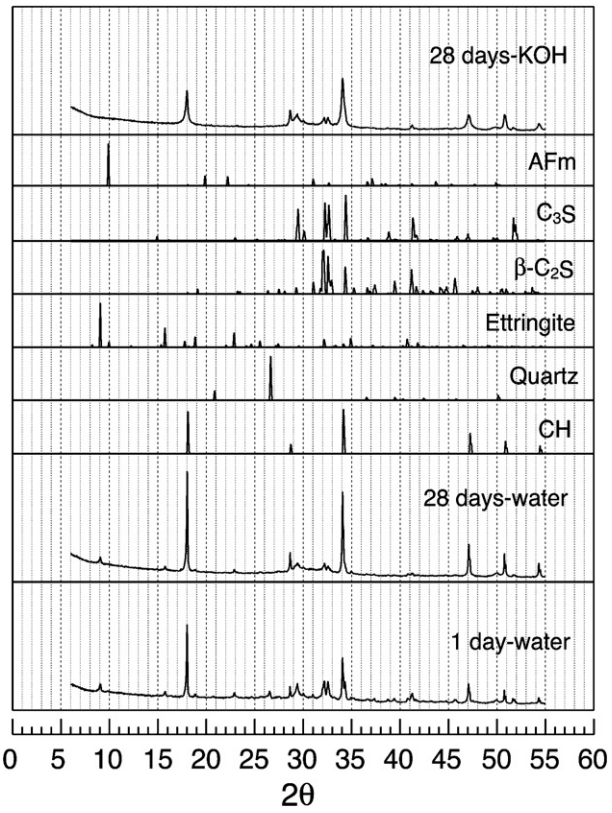

Fig. 1. XRD traces for both the 1 and 28-day-old water-activated pastes and the 28-day-old KOH-activated paste. Schematic X-ray powder diagrams are included for relevant phases.

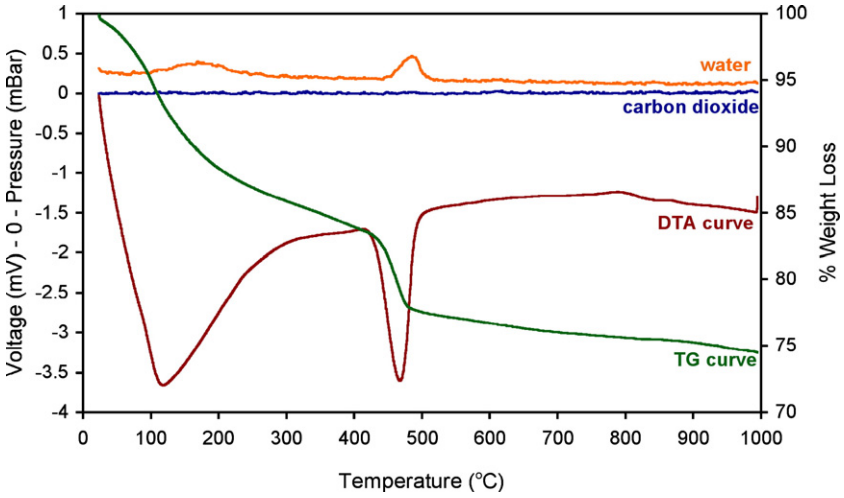

Fig. 2. Thermal analysis data for the 28-day-old water-activated paste.

an SEM (CamScan Series 4, U.K., equipped with an UTW EDX detector, Oxford, U.K., and ISIS software for imaging/X-ray analysis, Oxford Instruments) at an accelerating voltage of 20 kV and working distance of 28 mm. The images in this article were obtained using a Philips XL-30 SEM operated at 20 kV and at working distances between 7.7 and 10.7 mm.

Transmission electron microscopy with energy dispersive X-ray analysis (TEM–EDX) was used to examine the morphology of the C–S–H and to determine its chemical composition (Philips CM20, Eindhoven, Netherlands, equipped with an UTW EDX detector, Oxford, U.K., and ISIS software for imaging/X-ray analysis, Oxford Instruments). For TEM, 200 μm-thick slices were hand thinned, using silicon carbide paper of different grades (600–2400 grit from Struers, Glasgow, UK), until they were approximately 30 μm thick. Ni grids with a 2 × 1 mm slot were glued onto both sides of the sample as a 'sandwich'. The specimens were then argon ion-beam milled (Model 1010 Ion Mill, Fischione Instruments, PA, U.S.A.) using a liquid nitrogen cooled stage in order to avoid excessive specimen heating and consequent damage. The specimens were carbon coated after milling. Around 80 EDX analyses were taken of regions in each of the 28-day-old samples. Each region was checked before EDX analysis by selected area electron diffraction (SAED) for the presence of crystalline phases. This strategy ensured that analyses were obtained of C–S–H free of intermixture with other phases, except AFt, which is sufficiently unstable in the microscope that it loses structural order and consequently gives no crystalline reflections (i.e. spots) on the electron diffraction pattern; mixtures of C–S–H with AFt were therefore identified on the basis of morphology and compositional trends and such analyses were excluded when calculating mean compositions for C–S–H.

3. Results and discussion

3.1. X-ray diffraction and thermal analysis

Fig. 1 shows XRD traces from slices of the 1 and 28-day-old water-activated pastes and the 28-day-old KOH-activated paste. The data are all plotted with the same intensity scales. Schematic X-ray diagrams are included for relevant phases. The crystalline phases present in the 1-day-old water-activated paste include some residual alite and belite, CH and AFt. By 28 days, only a small amount of cement remains unreacted; the main crystalline hydration products are still CH and AFt with AFm not present in a sufficiently large quantity or with sufficiently large or ordered crystals to be detected by the technique. Activation with KOH resulted in a similarly high degree of reaction of the cement at 28 days. There are no peaks for AFm or AFt and those for CH are broad, indicating a small average crystal size, as observed previously in other KOH-activated systems [e.g. [14]].

The XRD data were complemented by thermal analysis techniques, including identification of the evolved gases. Illustrative data are shown in Fig. 2, which are for the water-activated paste hydrated for 28 days. The loss of mass below around 400 °C is due to the decomposition of the C–S–H and AFt phases, and the sharp loss between 400 and 500 is due to CH. The mass spectroscopy data at the top of the figure show unequivocally that the paste had not carbonated, in agreement with the absence from the XRD trace of peaks for any of the polymorphs of calcium carbonate. The quantities of CH in the pastes determined from the thermogravimetry curves are given in Table 2 (as percentage of ignited weight). At both 1 and

Table 2
Results from thermal analysis and the deconvolution of the single-pulse ^{29}Si NMR spectra for water- and KOH-activated samples hydrated for 1 and 28 days

	% WPC reacted	% CH	Al/Si	MCL	B (%)	B_{water}/B_{KOH} (%)
1 day water	58	21	0.06	3.5	38	61
1 day KOH	58	25	0.10	3.5	62	
28 days water	90	27	0.10	6.5	38	83
28 days KOH	93	35	0.10	5.2	46	

MCL = mean aluminosilicate chain length for C–S–H. B = bridging tetrahedra occupied by Al / bridging tetrahedra occupied by Al and Si. %CH = calcium hydroxide as % of ignited weight determined by thermogravimetry.

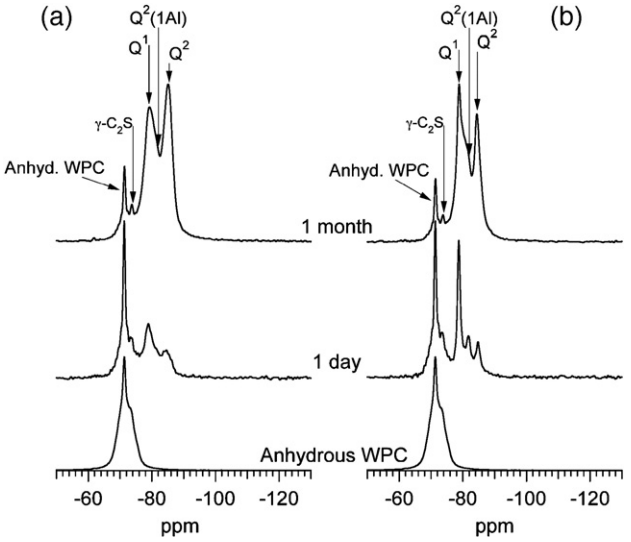

Fig. 3. Single-pulse ^{29}Si MAS NMR spectra for the anhydrous cement (bottom), and KOH-activated (right) and water-activated (left) pastes hydrated for 1 (middle) and 28 days (top). All spectra are scaled to their tallest peak. The chemical shifts of the hydrate peaks (in ppm) in the order Q^1, Q^2(1Al), Q^2(0Al) are: −78.8, −81.8, −84.8 for 1 day-KOH; −78.8, −81.2, −84.5 for 28 day-KOH; −78.9, −81.4, −84.7 for 1 day-water; −78.9, −81.1, −85.1 for 28 day-water.

28 days, KOH activation has resulted in a greater amount of CH than water activation.

3.2. ^{29}Si NMR of pastes hydrated for 1 day and 28 days

Fig. 3 shows the single-pulse ^{29}Si NMR spectra for the anhydrous WPC and for both the water- and KOH-activated pastes after 1 and 28 days hydration. Single-pulse ^{29}Si MAS NMR provides quantitative information on the fractions of Si present in different tetrahedral environments, Q^n, where n denotes the connectivity of the silicate tetrahedron: thus Q^0 represents isolated tetrahedra such as the ones present in the anhydrous WPC (Fig. 3, bottom, which is a convolution of a sharp peak component from belite (at −71 ppm) and a broader peak component from alite [16]); Q^1 represents chain-end group tetrahedra, with typical chemical shift at around −79 ppm; Q^2 represents middle-chain groups where both adjacent tetrahedra are occupied by silicon (shift at around −85 ppm) and Q^2(1Al) represents middle-chain groups where one of the adjacent tetrahedra is occupied by aluminium (which results in a down-field shift of around 3 ppm, giving a typical value of −82 ppm); Q^3 represents branching sites and Q^4 cross-linking sites in a three dimensional framework. As in previous studies [12–14] activation with KOH led to better-resolved peaks for

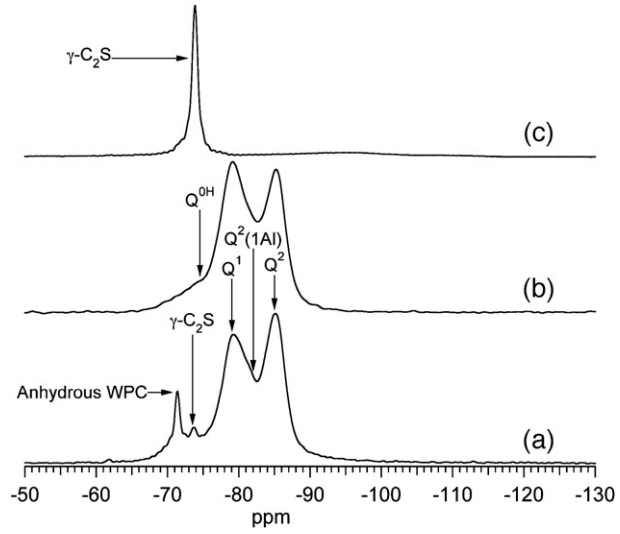

Fig. 4. Single-pulse ^{29}Si MAS NMR spectra for the water-activated paste hydrated for 28 days (a) and γ–C_2S (c) and a ^{1}H–^{29}Si CP MAS NMR spectrum for the paste (b). All spectra are scaled to their tallest peak.

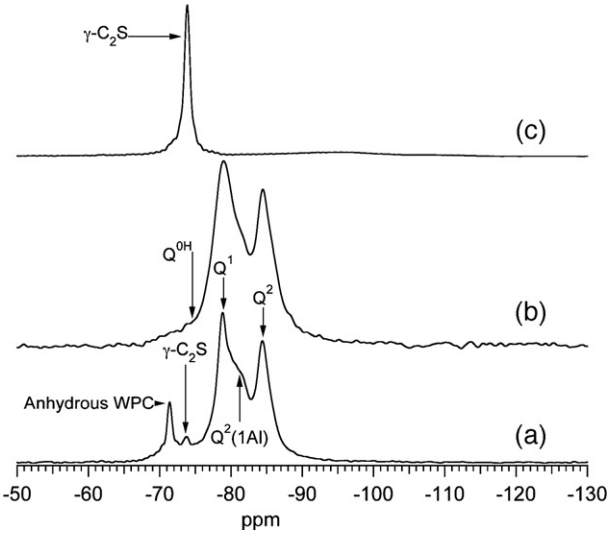

Fig. 5. Single-pulse ^{29}Si MAS NMR spectra for the KOH-activated paste hydrated for 28 days (a) and γ-C_2S (c) and a ^{1}H–^{29}Si CP MAS NMR spectrum for the paste (b). All spectra are scaled to their tallest peak.

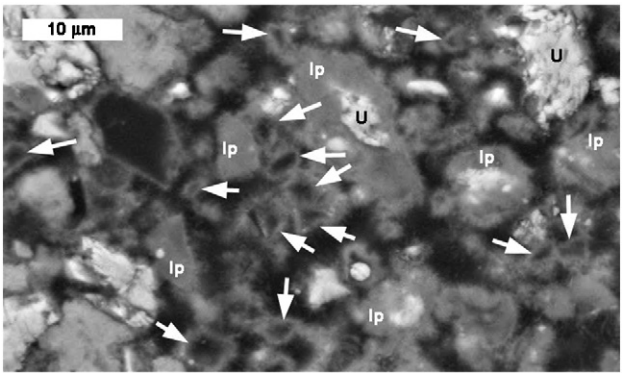

Fig. 6. Backscattered electron micrograph of an area in the 1-day-old water-activated paste. Regions of unreacted cement (U) and inner product C–S–H (Ip) are labelled. There are a number of small fully hydrated particles with dense rims, which are indicated with white arrows; comparison with resin-filled pores shows that the particles contains material, which is presumably low-density inner product C–S–H. Fibrils of outer product C–S–H can be seen protruding into the large pores.

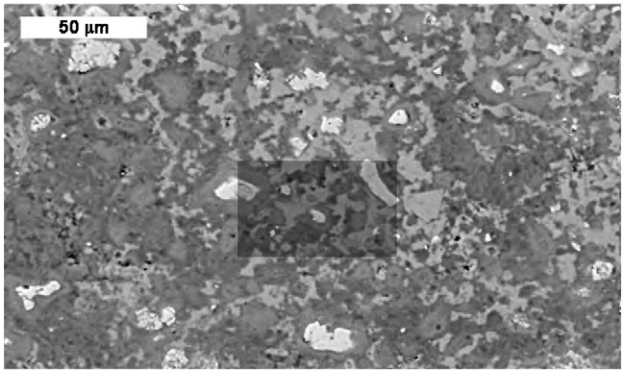

Fig. 7. A low magnification backscattered electron micrograph of an area in the 28-day-old water-activated blend, illustrating the paste's dense microstructure. The darker shaded rectangular area is shown at higher magnification in Fig. 8.

C–S–H indicating a greater degree of structural order. The results of the deconvolution of the spectra are given in Table 2. The amount of cement reacted at both ages studied was essentially the same with both water- and KOH-activation (i.e. around 60% at 1 day and around 90% at 28 days).

The mean length of the aluminosilicate anions (represented by the mean chain length, MCL, in Table 2) in the C–S–H after hydration for 1 day (58% reaction) is 3.5 with both water- and KOH-activation; that is, dimeric species are predominant. After 28 days – when most of the cement has reacted – the MCL has increased in both cases: to 6.5 with water and 5.2 with KOH, indicating that the aluminosilicate chains are either mainly pentameric, or mixtures of dimers with longer chains. The proportion of occupied bridging sites in the dreierkette chains that are occupied by Al^{3+} and not Si^{4+} remains unchanged between 1 and 28 days with water activation (at 38%) but reduces with KOH activation (from 62 to 46%). As a consequence the ratio of B_w/B_{KOH} is 61% at 1 day and 83% at 28 days; in other words, at one day, KOH activation produces around 1.6 times as much aluminium substitution as does water, and at 28 days it produces around 1.2 times (the Al/Si ratios are the same but the MCL is shorter with KOH). Interestingly, these values fall either side of the value observed previously for ground granulated blast-furnace slag/WPC blends with 50 and 90% slag – which had 1.3 times as much substitution with KOH [12] – and are the same as those for a metakaolin (MK)/WPC blend containing 20% MK [14], despite having very different Al/Si ratios and mean aluminosilicate chain lengths.

Fig. 4 again shows the single-pulse spectrum for the 28-day-old water-activated paste (a), together with a ^1H–^{29}Si cross polarization (CP) spectrum (b) and a spectrum for a synthetic γ-C_2S (c) (produced during previous work [17]). An additional sharp Q^0 peak centred at -73.5 ppm on the SP spectrum does not occur on the CP spectrum (b), where only hydrated structural units are detected, so the peak must be assigned to an anhydrous structural unit. Following previous studies [17–21] this peak is assigned here to γ-C_2S, and an experimental spectrum acquired during this work from a sample of synthetic γ-C_2S is consistent with this assignment (Fig. 4 (c)). The same peak is present on the SP spectrum for the KOH-activated paste, Fig. 5.

The two ^1H–^{29}Si CP spectra (Figs. 4(b) and 5(b)) both show that hydrated monomeric units are present, and that there is probably less in the KOH-activated system than in that with water, which would be consistent with previous work (see Discussion in [22]).

3.3. Backscattered electron imaging with X-ray analysis

The microstructure of the water-activated sample was quite porous after one day of hydration, with areas of CH, partially reacted cement particles (that were often surrounded by Ip C–S–H), and many small fully reacted particles. An illustrative BSE micrograph of an area in the 1-day-old paste is shown in Fig. 6, which includes some labelled examples of unreacted material (U) and inner product C–S–H (Ip). Whilst some of the fully reacted particles appeared to be hollow, most contained some product, probably a low-density Ip C–S–H (as observed previously in many systems by TEM (see for example [13]); examples are indicated by white arrows on Fig. 6.

After hydration for 28 days, the water-activated sample had a much denser microstructure due to the formation of more outer product (Op) C–S–H due to the greater extent of cement hydration. An illustrative micrograph is shown in Fig. 7. A region in the middle of the micrograph – indicated by a darker shaded rectangular area – is shown at higher magnification in Fig. 8, which includes labels for unreacted cement (U), calcium hydroxide (CH), outer product C–S–H (Op) and dense inner product C–S–H (Ip).

An attempt was made to determine the chemical composition of C–S–H in the samples by EDX analysis in the SEM; points were selected for statistical analysis on the basis of compositional trends and microstructural location. The data for the 28-day-old samples with both water- and KOH-activation are plotted as Al/Ca against Si/Ca atom ratio scatter diagrams in Fig. 9; mean Ca/Si and Al/Si ratios for both 1 and 28 days are given in Table 3. The mean Ca/Si ratios for the water-activated system are very similar to values found previously using the same technique by Escalante-Garcia and Sharp [7] for Ip C–S–H present in two ordinary Portland cements with w/c of 0.5 hydrated

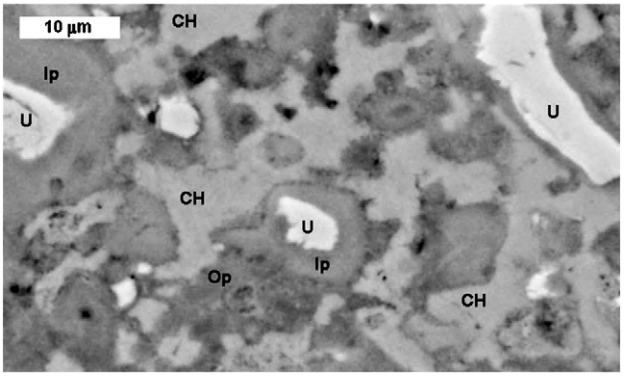

Fig. 8. A backscattered electron micrograph that illustrates an area of dense microstructure (part of Fig. 7 at higher magnification). Regions of calcium hydroxide (CH), unreacted cement (U), Op C–S–H (Op) and dense inner product C–S–H (Ip) are labelled.

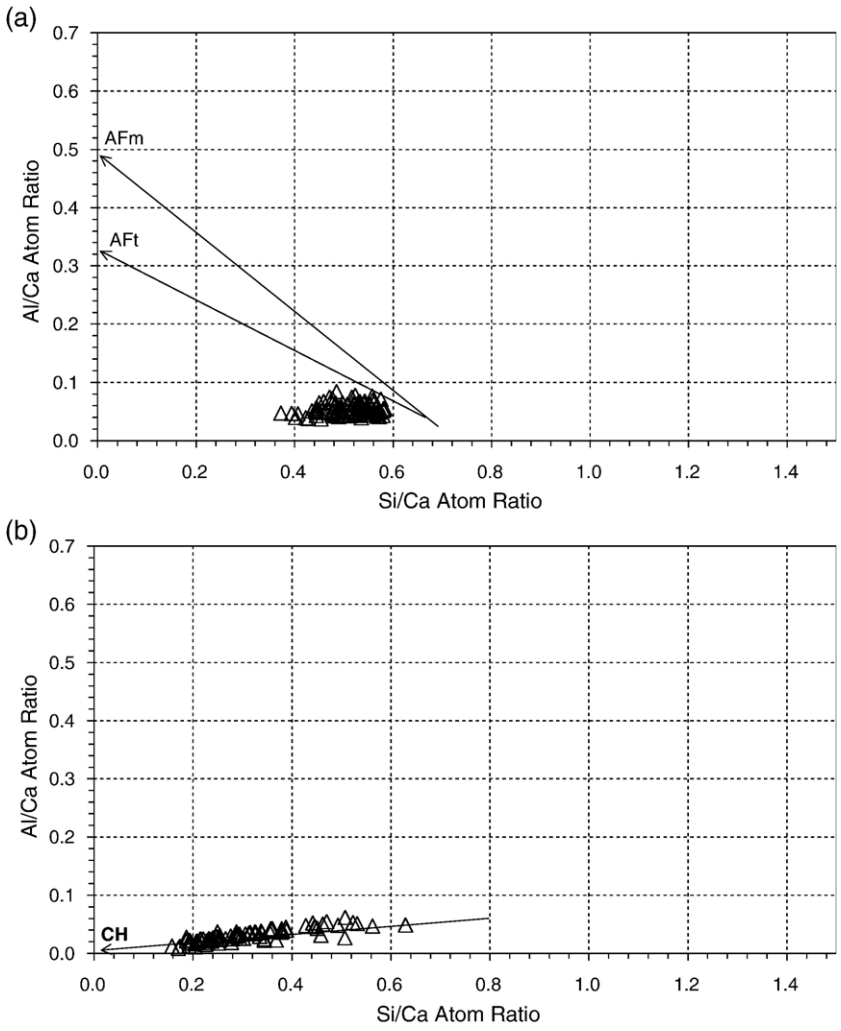

Fig. 9. Al/Ca against Si/Ca atom ratio plots of SEM–EDX analyses of 'C–S–H' present in the water-activated (a) and KOH-activated (b) pastes hydrated for 28 days (see Discussion and Fig. 15 for relevance of the tie-lines).

at 60 °C and by Kjellsen [5] for both Ip and Op C–S–H in an OPC-based high performance concrete (containing 5% silica fume) with water/binder ratio of 0.31 hydrated at 50 °C; the distribution of the data in Fig. 9(a) is, for example, similar to those in Fig. 2 of [7]. They are, however, at the high end of values measured previously by TEM for C–S–H in Portland cement pastes hydrated at lower temperature (20 °C) [23] and those for the KOH-activated system are much higher than is possible to achieve for C–S–H in models for the structure of C–S–H (see Discussion in [22]). Interestingly, the data for the KOH-activated paste (Fig. 9(bottom)) are distributed along a straight line towards the origin, indicating various levels of inter-mixture between C–S–H and CH. These SEM–EDX data are compared in Section 3.4 with the compositions determined by TEM–EDX of C–S–H generally free of intermixing with other phases.

The grey level of C–S–H in the water-activated paste was in places quite similar to the CH: that is, it was brighter than in pastes cured at lower temperature, an observation that is in agreement with previous studies [3,6,11].

3.4. Transmission electron microscopy with X-ray analysis

Samples of both the water- and KOH-activated pastes that had been hydrated for 28 days were examined by TEM. Much of the Ip C–S–H in the water-activated paste has the fine scale homogeneous morphology that has been observed previously in cements hydrated at 20 °C (for examples see [23]); a typical example is shown in Fig. 10 (below the line indicated by the white arrows, which represents the interface between Op and Ip). The

Table 3
Mean Ca/Si and Al/Si atomic ratios obtained for 'C–S–H' using SEM–EDX (S.D. = standard deviation; N = number of analyses)

	1 day				1 month			
	Wwpc	S.D.	Kwpc	S.D.	Wwpc	S.D.	Kwpc	S.D.
		N=82		N=74		N=98		N=101
Ca/Si	2.12	0.51	3.45	1.38	1.97	0.20	3.46	1.10
Al/Si	0.13	0.03	0.11	0.03	0.11	0.02	0.10	0.02

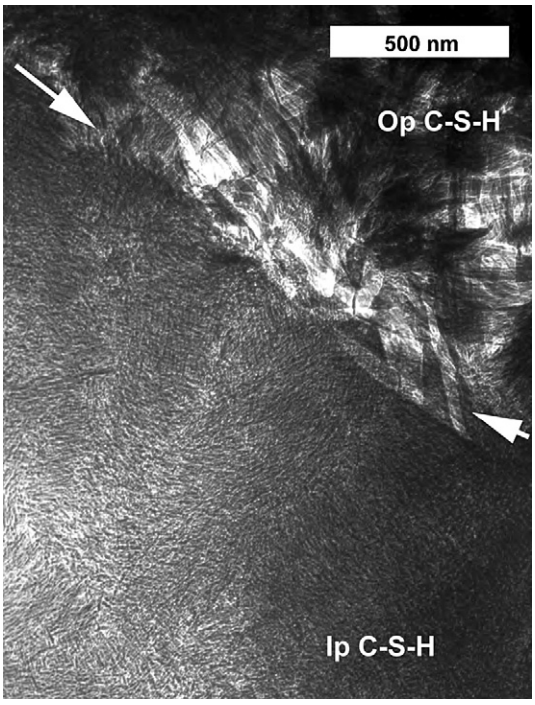

Fig. 10. A TEM micrograph from the water-activated paste hydrated for 28 days showing fibrillar Op C–S–H (with relicts of AFt) and fine Ip C–S–H; the interface between Ip and Op is indicated with white arrows.

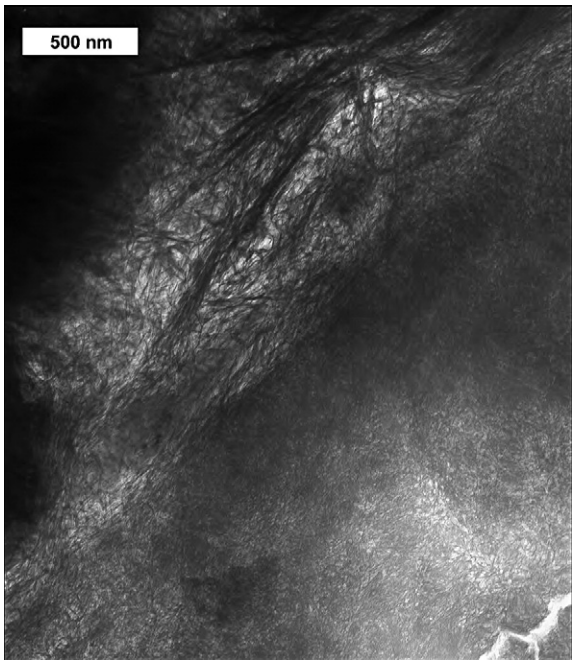

Fig. 12. A TEM micrograph from the KOH-activated paste hydrated for 28 days showing foiland lath-like Op C–S–H (top and left) and very fine Ip C–S–H (bottom and right). The interface between Ip and Op runs from the bottom left corner to the top right.

Op C–S–H is also similar to that formed at lower temperatures in being essentially fibrillar, although often somewhat coarser, which is consistent with previous observations at higher temperature [24]. Examples of coarse fibrillar C–S–H are shown in Fig. 11, although it is not entirely clear whether these examples are Op or Ip because of their spatial relationship with other Op and Ip C–S–H in the micrograph that have well-established morphologies (i.e. the fine fibrillar Op C–S–H that is directly below the labelled coarse C–S–H, and the fine Ip C–S–H that is to the right of the coarse C–S–H that is in the bottom left corner). Figs. 10 and 11 also contain examples of relicts of AFt

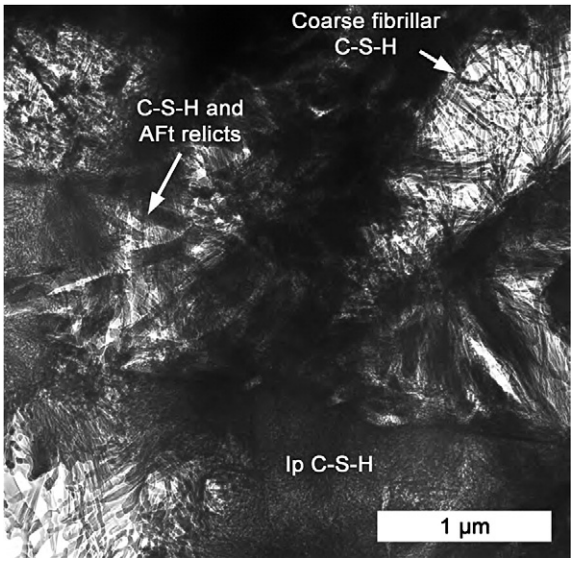

Fig. 11. A TEM micrograph from the water-activated paste hydrated for 28 days showing coarse fibrillar C–S–H (indicated and bottom left), fine fibrillar Op C–S–H (both below the labelled coarse C–S–H and mixed with relicts of AFt), and fine Ip C–S–H.

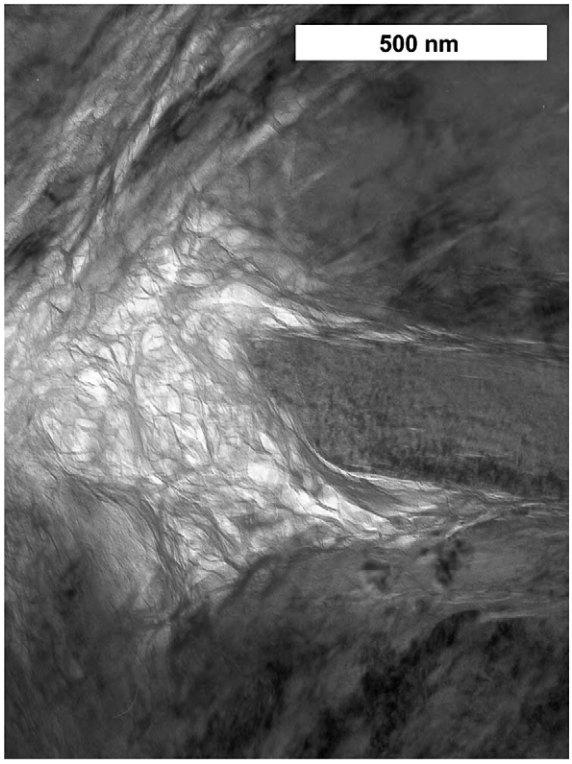

Fig. 13. A TEM micrograph from the KOH-activated paste hydrated for 28 days showing microcrystalline CH intermixed with C–S–H and foil-like Op C–S–H (centre-left).

Fig. 14. A TEM micrograph from the KOH-activated paste hydrated for 28 days showing foiland lath-like Op C–S–H.

intermixed with Ip and fine fibrillar Op C–S–H. For example, the linear features that are immediately to the left of the point of the arrow on the right-hand side of Fig. 10 are AFt relicts; the presence of AFt at Ip/Op interfaces is a common observation (for another example, see Fig. 4 of reference [23]).

The Ip C–S–H present in the KOH-activated paste also has a very fine homogeneous morphology; an example is shown in Fig. 12. The morphology of Op C–S–H that is formed with KOH activation is – as observed at 25 °C [12] – foil- and lath-like rather than fibrillar. Good illustrative examples of both morphologies are shown in Figs. 12–14: foil- and lath-like in 12 and 14 and foil-like only in 13. The laths appear to consist of stacks of very poorly ordered layers, which merge with the crumpled foils. The microcrystalline nature of CH in the KOH-activated paste indicated by XRD (Fig. 1) was confirmed by TEM; an example is shown in Fig. 13 where the CH microcrystals appear dark where they are oriented such that they diffract electrons strongly. This is a typical feature of KOH-activated systems, as previously reported for pastes of neat WPC and slag-WPC blends [12] and a metakaolin-WPC blend [14] hydrated at 25 °C. Microcrystalline CH intermixed with C–S–H has not been observed in water-activated PC pastes of normal w/c ratio hydrated at 20 to 25 °C. Whilst such fine intermixing has been observed in pastes hydrated at 80 °C [22] it was not observed in this study at 55 °C.

EDX analyses were taken from areas of Ip and Op C–S–H approximately 200 nm in diameter, in both the water and KOH-activated pastes. Analyses for the water-activated paste are plotted in Figs. 15–17, and analyses for the KOH-activated paste are plotted in Figs. 18–20. It was sometimes difficult in the water-activated paste to select areas totally free of relicts of AFt, which, because they are partially decomposed, cannot be discarded on the basis of the presence of crystalline reflections on a SAED pattern. The difficulty can be appreciated by examining the Op regions in Figs. 10 and 11 where fibrillar Op C–S–H is intermixed with relicts of AFt; for example, the linear striation running upwards from the tip of the right-hand arrow on Fig. 10 is an AFt relict. Analyses of such mixtures will of course contain enhanced amounts of Ca, Al and S, as is evident on the scatter plots in Figs. 15 and 16; such analyses were excluded when calculating mean compositions for the C–S–H. The two analyses of Op C–S–H that have the highest Al/Ca ratio, together with a number of analyses of Ip C–S–H, also appear to include a contribution from microcrystals of a hydrotalcite-like phase (i.e. a Mg,Al double hydroxide phase,

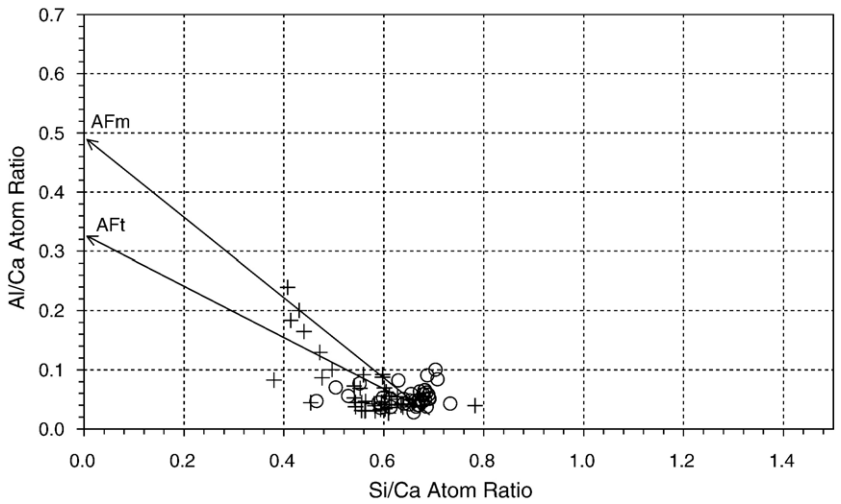

Fig. 15. Al/Ca against Si/Ca atom ratio plot of TEM–EDX analyses of Op (+) and Ip (○) C–S–H present in the water-activated paste hydrated for 28 days.

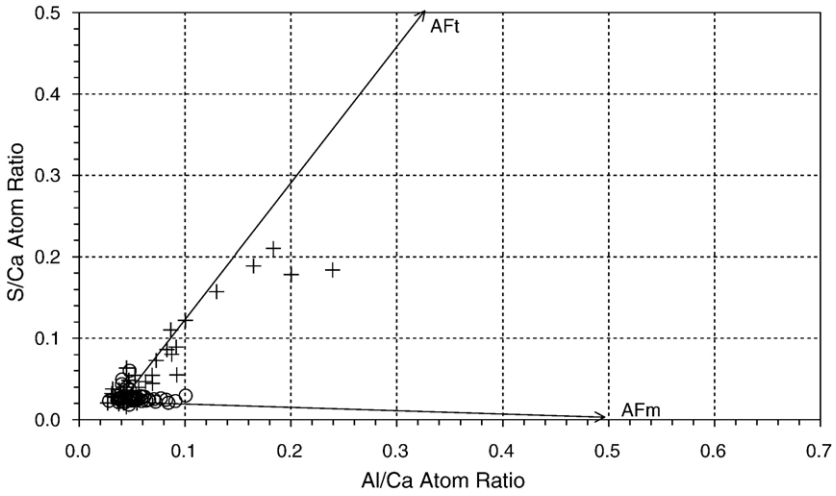

Fig. 16. S/Ca against Al/Ca atom ratio plot of TEM–EDX analyses of Op (+) and Ip (○) C–S–H present in the water-activated paste hydrated for 28 days.

which can contain various interlayer anions), as indicated on Fig. 17.

Relicts of AFt crystals were not observed in the KOH-activated specimen, in agreement with recent work on a metakaolin-WPC blend activated with KOH [14]. As a consequence, the Al/Ca against Si/Ca and S/Ca against Al/Ca plots in Figs. 18 and 19 show that none of the analyses contain contributions from AFt. Whilst AFm phases can occur in KOH-activated cements [15], there is no contribution from such a phase in these data. The higher S/Ca values in Fig. 19 are clearly associated with enhanced K/Ca, Fig. 20; indeed the K/Ca and S/Ca values increase in an approximate 2:1 ratio, which suggests strongly that SO_4^{2-} ions are adsorbed on the C–S–H balanced by K^+ ions. The regression line indicates that the C–S–H itself has a K/Ca ratio of 0.09.

Mean values of Ca/Si, Ca/(Al+Si) and Al/Si ratios for both Ip and Op C–S–H are given in Table 4. There is no statistically significant difference between the Al/Si ratios of the Ip and Op C–S–H with both water and KOH activation and the values measured in the TEM are in good agreement with those determined by deconvolution of the NMR spectra. In contrast, the Ca/Si and Ca/(Al+Si) ratios of the Ip C–S–H are in both cases statistically significantly lower than those of the Op C–S–H. The mean value of the Ca/(Al+Si) ratio of the C–S–H present in the KOH-activated paste (1.33) is also significantly lower than with water activation (1.50), which is consistent with the lower amount of CH in the water-activated paste (Table 2).

It was noted in Section 3.3 that the Al/Ca against Si/Ca ratio plot for the water-activated paste is very similar to SEM–EDX data reported previously by Escalante-Garcia and Sharp for Ip C–S–H [7]. Those authors considered that such clusters of analyses corresponded to essentially pure C–S–H. However, comparison of the SEM–EDX data in Fig. 9(a) with the TEM–EDX data in Fig. 15 shows that in this case it is unlikely that the cluster in Fig. 9(a) is due solely to C–S–H; the difference between the mean values for the Ca/Si ratios determined by SEM–EDX and TEM–EDX is statistically extremely

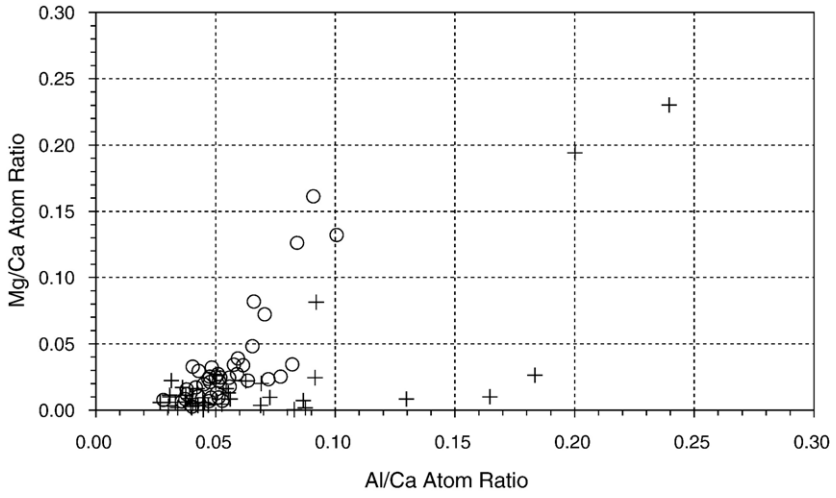

Fig. 17. Mg/Ca against Al/Ca atom ratio plot of TEM–EDX analyses of Op (+) and Ip (○) C-SH present in the water-activated paste hydrated for 28 days.

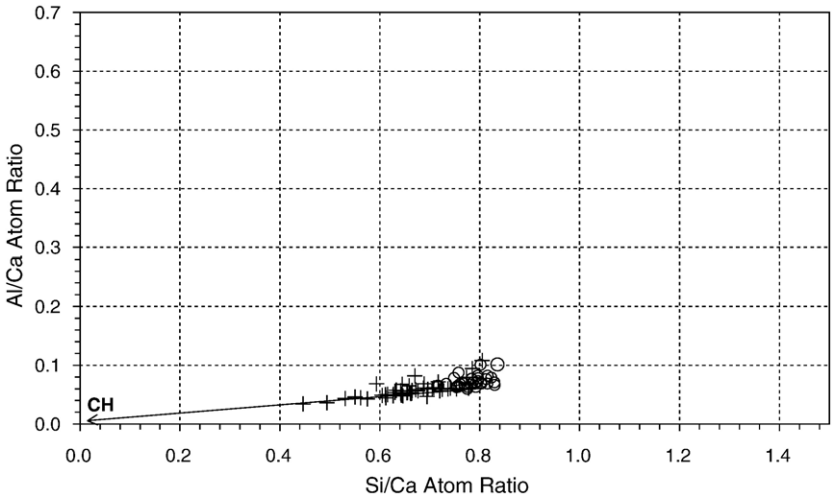

Fig. 18. Al/Ca against Si/Ca atom ratio plot of TEM–EDX analyses of Op (+) and Ip (○) C–S–H present in the KOH-activated paste hydrated for 28 days.

significant, so the SEM data would appear to be due to C–S–H intermixed with other phases, in particular CH: that is, that many crystals of CH and other hydration products are sufficiently small compared with the size of the X-ray generation volume – and evenly distributed – that the intermixture of phases results in the cluster of analyses observed by SEM–EDX, which understandably could be interpreted as being due to 'pure' C–S–H. Regarding the KOH-activated paste, intuitively, one would expect the smaller average crystal size of the CH to lead to a smaller cluster in the SEM–EDX data than with water activation. However, in contrast to the water-activated paste, almost all the CH in the KOH-activated paste is in fact intimately mixed with C–S–H, ranging from small microcrystals embedded in C–S–H to large CH-rich regions that have small amounts of C–S–H interstratified between layers of CH; such intermixing results in the wide range of Si/Ca ratio observed in both the SEM–EDX and TEM–EDX data, Figs. 9(b) and 18 respectively.

3.5. Structural-chemical formulae for C–S–H

The TEM–EDX and NMR data in Tables 2 and 4 can be used to establish formulae for average structural units in the C–S–H in terms of the two alternative formulations for the nanostructure of C–S–H given by Richardson and Groves [22,25,26]; i.e. in terms of either the tobermorite-jennite (T/J) or tobermorite-calcium hydroxide (T/CH) structural viewpoints. The T/J viewpoint envisages C–S–H to consist of structural elements based on the crystalline minerals 1.4 nm tobermorite (T) and jennite or jaffeite (J), whilst the T/CH viewpoint envisages elements of tobermorite-based structure interstratified with layers of CH-based structure. The models are discussed and illustrated in detail in reference [22]. The procedure to establish the structural formulae is straightforward: it simply involves calculation of the models' variables by inserting the experimentally determined mean values of Ca/Si and Al/Si ratios and aluminosilicate chain length into the formulae given

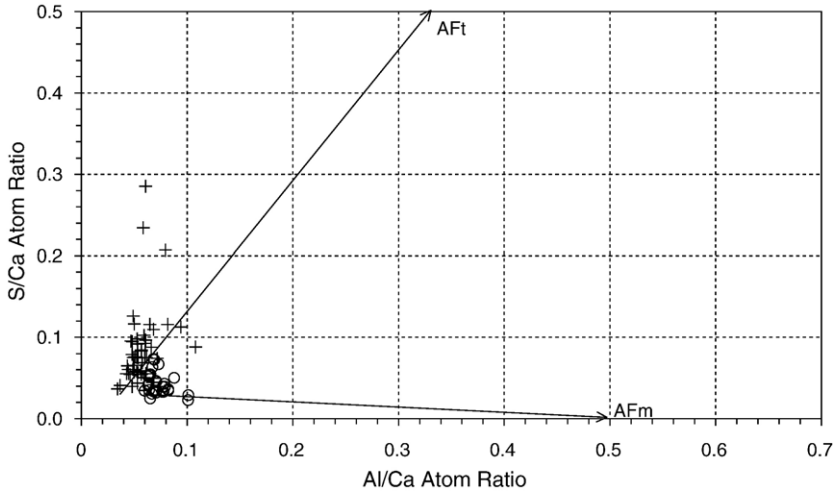

Fig. 19. S/Ca against Al/Ca atom ratio plot of TEM–EDX analyses of Op (+) and Ip (○) C–S–H present in the KOH-activated paste hydrated for 28 days.

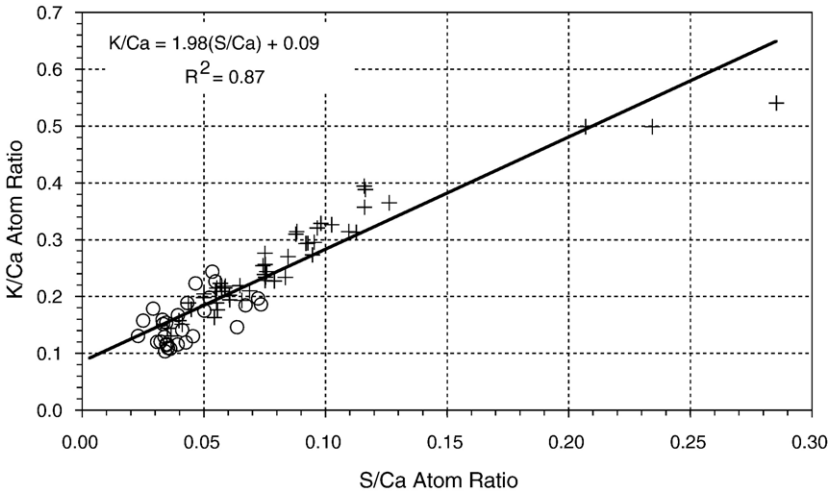

Fig. 20. K/Ca against S/Ca atom ratio plot of TEM–EDX analyses of Op (+) and Ip (○) C–S–H present in the KOH-activated paste hydrated for 28 days. Note that whilst on inspection it is clear that the data would follow a different trend line if the three data points with the highest S/Ca and K/Ca ratios were excluded from the regression analysis, there was no morphological or structural reason to discard them (and the quality of fit is not improved by doing so).

in [12] and [15] (and summarized in [22]); the values of the variables calculated using the data reported in this article are given in Table 5. So, for example, for the 28-day-old water-activated paste, an average structural unit with minimum degree of protonation of the aluminosilicate chains and assuming that the substitution of Si^{4+} by Al^{3+} is balanced entirely by Ca^{2+} ions, can be represented by (1):

$$\{Ca_5(Si_{0.91}Al_{0.09})_{6.5}O_{20.5}\}\cdot(OH)_{3.7}\cdot Ca_{4.6}\cdot mH_2O \quad (1)$$

The presence of hydroxyl groups outside the braces indicates that in terms of the T/J viewpoint, there must be some J-like structure: with zero protonation of the chains, totally J-like structure would be present if $y'=6$ (see [12] or [22] for the definition of y'), whereas the experimental data give a value of 3.5, so in this case there would be both T- and J-like structure present.

In terms of the T/CH viewpoint, the average structural unit is represented by (2):

$$Ca_{7.5}(Si_{0.91}Al_{0.09})_{6.5}O_{20.5}\cdot Ca_{0.3}\cdot 1.84Ca(OH)_2\cdot mH_2O \quad (2)$$

Unfortunately, it is not possible to decide from the data presented in this article which of these two structural viewpoints, T/J or T/CH, is most appropriate for the C–S–H present in the water-activated paste.

Repeating the same procedure for the KOH-activated paste – again assuming minimum degree of protonation of the aluminosilicate chains – but this time assuming that substitution of Si^{4+} by Al^{3+} is charge balanced entirely by K^+ ions, an average structural unit is represented by (3):

$$\{Ca_{4.13}(Si_{0.91}Al_{0.09})_{5.2}O_{16.6}\}\cdot K_{0.47}\cdot(OH)_{1.21}\cdot Ca_{2.67}\cdot mH_2O \quad (3)$$

The presence of hydroxyl groups outside the braces again indicates that on the T/J viewpoint there must be some J-like structure. However, in this case, the distribution of TEM–EDX data (Fig. 18) indicates very clearly that the T/CH viewpoint is more applicable than the T/J, so the formula for an average structural unit is more appropriately represented by (4):

$$Ca_{6.2}(Si_{0.91}Al_{0.09})_{5.2}O_{16.6}\cdot K_{0.47}\cdot 0.61Ca(OH)_2\cdot mH_2O \quad (4)$$

Interestingly, the K/Ca ratio in this formula – which is 0.07 – is very similar to the ratio given by the regression equation in Fig. 20 at S/Ca=0, thus indicating that the potassium in the KOH-activated paste was present either within the C–S–H structure charge balancing the substitution of Al^{3+} for Si^{4+}, or adsorbed on the C–S–H charge balancing sulfate ions (i.e. a K/S ratio of 2).

Table 4
Mean Ca/Si, Ca/(Al+Si) and Al/Si atom ratios for both Op and Ip C–S–H in one-month-old samples obtained using TEM–EDX and Al/Si atom ratios determined by deconvolution of the single-pulse ^{29}Si MAS NMR spectra (S.D. = standard deviation; N = number of analyses)

		N	Ca/Si		Ca/(Al+Si)		Al/Si		
			Mean	S.D.	Mean	S.D.	Mean	S.D.	NMR
Wwpc	Op	35	1.72	0.16	1.58	0.13	0.09	0.04	0.10
	Ip	40	1.56	0.16	1.44	0.15	0.08	0.02	
	All	75	1.63	0.18	1.50	0.16	0.09	0.03	
Kwpc	Op	48	1.54	0.19	1.42	0.18	0.09	0.01	0.10
	Ip	30	1.28	0.05	1.17	0.05	0.09	0.01	
	All	78	1.44	0.20	1.33	0.19	0.09	0.01	

Table 5
Values of variables in Richardson and Groves' model for C–S–H in the 28-day-old samples calculated using the NMR and TEM–EDX data in Tables 2 and 4; see [22] and references therein for details of the model

	a	n	y	y'	w_{min}	w_{max}	X	z
Wwpc	0.091	2.500	3.705	3.469	0	5.00	7.50	1.84
Kwpc	0.091	2.067	2.587	2.359	0	4.14	6.20	0.61

The NMR-derived Al/Si ratios were used to calculate a; the values of y correspond to the assumption that the substitution of Si^{4+} by Al^{3+} is charge compensated entirely by alkali cations and y' to compensation by Ca^{2+} ions; the values of X and z correspond to the minimum degree of protonation of the aluminosilicate chains (i.e. for w_{min}).

4. Conclusions

The microstructure and composition of water- and alkali-activated hardened pastes of white Portland cement hydrated at 55 °C have been characterized using a multi-technique approach, with particular emphasis on the nature of the C–S–H phase. The amount of cement reacted at both ages studied was essentially the same with both water- and KOH-activation (i.e. around 60% at 1 day and around 90% at 28 days). The main crystalline hydration products were CH and AFt with water activation, and CH only with alkali; the CH formed in the alkali-activated system had a small average crystal size. Alkali activation resulted in C–S–H with slightly more structural order than with water. After 1-day hydration, the mean length of the aluminosilicate anions in the C–S–H was 3.5 with both methods of activation, and increased to 6.5 and 5.2 by 28 days with water and alkali respectively. Inner product C–S–H with a fine scale, homogeneous morphology, was abundant in both systems. Outer product C–S–H was generally fibrillar with water, and foil- or lath-like with alkali, both of which are consistent with previous observations at lower temperature. The higher temperature curing did, however, result in some regions of coarser morphology. It was not possible to determine the chemical composition of C–S–H free of intermixture with other phases by X-ray analysis in the SEM; the higher resolution of TEM–EDX was necessary. The C–S–H formed in the alkali-activated paste had a lower mean Ca/(Al+Si) ratio than that formed with water, which was offset by a larger quantity of calcium hydroxide. In both systems, inner product C–S–H had significantly lower Ca/Si and Ca/(Al+Si) ratios than outer product C–S–H. Good agreement was found between the mean values for the Al/Si atom ratios determined using TEM–EDX and MAS NMR. The potassium in the KOH-activated paste was present either within the C–S–H structure charge balancing the substitution of Al^{3+} for Si^{4+}, or adsorbed on the C–S–H charge balancing sulfate ions (i.e. a K/S ratio of 2).

Acknowledgements

Thanks are due to the Engineering and Physical Sciences Research Council for funding under Grant No. GR/S45874/01, to Jason Boomer at W.R. Grace for conducting the XRD experiments and to Castle Cement, UK Nirex Ltd., and Lafarge Cements for additional technical and financial support.

References

[1] H.F.W. Taylor, Cement Chemistry, 2nd ed., Thomas Telford Publishing, London, 1997.
[2] K.L. Scrivener, The effect of heat treatment on inner product C–S–H, Cem. Concr. Res. 22 (1992) 1224–1226.
[3] K.O. Kjellsen, R.J. Detwiler, O.E. Gjørv, Backscattered electron imaging of cement pastes hydrated at different temperatures, Cem. Concr. Res. 20 (1990) 308–311.
[4] Y. Cao, R.J. Detwiler, Backscattered electron imaging of cement pastes cured at elevated temperatures, Cem. Concr. Res. 25 (1995) 627–638.
[5] K.O. Kjellsen, Heat curing and post-heat curing regimes of high-performance concrete: Influence in microstructure and C–S–H composition, Cem. Concr. Res. 26 (1996) 295–307.
[6] J.I. Escalante-Garcia, J.H. Sharp, Effect of temperature on the hydration of the main clinker phases in Portland cements: Part I, Neat cements, Cem. Concr. Res. 28 (1998) 1245–1257.
[7] J.I. Escalante-Garcia, J.H. Sharp, Variation in composition of C–S–H gel in Portland cement pastes cured at various temperatures, J. Am. Ceram. Soc. 82 (1999) 3237–3241.
[8] J.I. Escalante-Garcia, J.H. Sharp, The microstructure and mechanical properties of blended cements hydrated at various temperatures, Cem. Concr. Res. 31 (2001) 695–702.
[9] R. Yang, J.H. Sharp, Hydration characteristics of Portland cement after heat curing: I, Degree of hydration of the anhydrous cement phases, J. Am. Ceram. Soc. 84 (2001) 608–614.
[10] R. Yang, J.H. Sharp, Hydration characteristics of Portland cement after heat curing: II, Evolution of crystalline aluminate-bearing hydrates, J. Am. Ceram. Soc. 84 (2001) 1113–1119.
[11] C. Famy, K.L. Scrivener, A.K. Crumbie, What causes differences of C–S–H gel grey levels in backscattered electron images, Cem. Concr. Res. 32 (2002) 1465–1471.
[12] I.G. Richardson, G.W. Groves, The structure of the calcium silicate hydrate phases present in hardened pastes of white Portland cement/blast-furnace slag blends, J. Mater. Sci. 32 (1997) 4793–4802.
[13] I.G. Richardson, The nature of C–S–H in hardened cements, Cem. Concr. Res. 29 (1999) 1131–1147.
[14] C.A. Love, I.G. Richardson, A.R. Brough, Composition and structure of C–S–H in white Portland cement-20% metakaolin pastes hydrated at 25 °C, Cem. Concr. Res. 37 (2007) 109–117.
[15] I.G. Richardson, A.R. Brough, G.W. Groves, C.M. Dobson, The characterization of hardened alkali-activated blast-furnace slag pastes and the nature of the calcium silicate hydrate (C–S–H) phase, Cem. Concr. Res. 24 (1994) 813–829.
[16] J.R. Barnes, A.D.H. Clague, N.J. Clayden, C.M. Dobson, C.J. Hayes, G.W. Groves, S.A. Rodger, Hydration of Portland cement followed by ^{29}Si Solid-State NMR spectroscopy, J. Mater. Sci. Lett. 4 (1985) 1293–1295.
[17] S.A. Rodger, The chemistry of admixture interaction during cement hydration, D.Phil. thesis, University of Oxford, 1986.
[18] M. Mägi, E. Lippmaa, A. Samoson, G. Engelhardt, A.-R. Grimmer, Solid-state high-resolution silicon-29 chemical shifts in silicates, J. Phys. Chem. 88 (1984) 1518–1522.
[19] A.-R. Grimmer, F. von Lampe, M. Mägi, E. Lippmaa, High-resolution solid-state ^{29}Si NMR of polymorphs of Ca_2SiO_4, Cem. Concr. Res. 15 (1985) 467–473.
[20] S.-H. Hong, J.F. Young, Hydration kintetics and phase stability of dicalcium silicate synthesized by the Pechini process, J. Am. Ceram. Soc. 82 (1999) 1681–1686.
[21] K.J.D. Mackenzie, M.E. Smith, Multinuclear Solid-State NMR of Inorganic Materials, Pergamon Materials Series, Elsevier Science Ltd, Oxford, 2002.
[22] I.G. Richardson, Tobermorite/jennite and tobermorite/calcium hydroxide-based models for the structure of C–S–H: applicability to hardened pastes of tricalcium silicate, β-dicalcium silicate, Portland cement, and blends of Portland cement with blast-furnace slag, metakaolin or silica fume, Cem. Concr. Res. 34 (2004) 1733–1777.
[23] I.G. Richardson, G.W. Groves, Microstructure and microanalysis of hardened ordinary Portland cement pastes, J. Mat. Sci. 28 (1993) 265–277.
[24] I.G. Richardson, Electron microscopy of cements, in: P. Barnes, J. Bensted (Eds.), Chapter 22 in Structure and Performance of Cements, 2nd ed., Spon Press, London, 2002, pp. 500–556.
[25] I.G. Richardson, G.W. Groves, Models for the composition and structure of calcium silicate hydrate (C–S–H) gel in hardened tricalcium silicate pastes, Cem. Concr. Res. 22 (1992) 1001–1010.
[26] I.G. Richardson, G.W. Groves, The incorporation of minor and trace elements into calcium silicate hydrate (C–S–H) gel in hardened cement pastes, Cem. Concr. Res. 23 (1993) 131–138.